



Full Length Article

Wallpapering-inspired spreading and wrinkling of atomically-thin materials

Sang Il Lee^a, Hyeong-Gyu Lim^b, Sun Sang Kwon^a, Su Han Kim^a, Jae Hyung Lee^a, Jeong-Min Park^a, Jae-il Jang^a, Sung Ik Yang^b, Won Il Park^{a,*}^a Division of Materials Science and Engineering, Hanyang University, Seoul 04763, Republic of Korea^b Department of Applied Chemistry, Kyung Hee University, Yongin-Si 17104, Republic of Korea

ARTICLE INFO

Keywords:

Graphene
Graphene wrinkle
Wrinkled graphene
Wrinkled membrane
Wrinkle-free graphene
Surface corrugation

ABSTRACT

We propose a novel wallpapering-inspired strategy to create wrinkles in a desired location and direction of single-layer graphene (Gr). The key to controlling the wrinkles is to regulate the permeation and release of solution through a regular array of holes between the substrate surface and Gr-based thin membrane (Gr/Cu in the first stage and Gr in the second stage). Microscopic analysis showed that neighboring holes were interconnected by straightened wrinkles with a width of 300–500 nm and height of 10–20 nm, while surface corrugations (e.g., ripples and wrinkles) were suppressed on the planar regions surrounded by wrinkles. Wrinkling mechanism was further verified by in-situ optical microscopy and comparative analysis of Gr/Cu ripples and Gr wrinkles. Our approach is simple yet universally applicable to diverse types of thin membranes, thereby offering a robust and versatile route to engineering properties of atomically thin materials.

1. Introduction

Wrinkling is a common phenomenon in thin membranes and can be found in the macroscopic world (e.g., Earth's mantle and wallpaper) as well as atomically-thin two-dimensional (2D) materials [1], such as graphene (Gr) [2–4]. It is well known that wrinkling occurs frequently in Gr during chemical-vapor-deposition (CVD) growth due to differences between the thermal expansion coefficient of Gr and the substrate [5]. In addition, a high density of ripples and wrinkles can be found when Gr is transferred onto other substrates [6]. Such surface corrugations are often considered to be undesirable imperfections that degrade the intrinsic properties of Gr, such as carrier mobility and electrical conductivity. Much effort has therefore been devoted to achieving wrinkle-free Gr; representative examples include CVD growth on substrates with a similar thermal expansion coefficient to Gr [7] and Gr transfer using volatile liquids with low surface tension [8].

However, new light has recently been shed on the potential of wrinkles in Gr [9–11]. Notably, these imperfections can modify electronic band structure [12–14], induce pseudo-magnetic fields and polarized carrier puddles [15], and provide additional mechanical flexibility [16,17], chemical reactivity [18], surface wettability [19,20], and heat resistivity [21–23]. To take full advantage of these opportunities, however, it is prerequisite to understand and control wrinkle formation in Gr. In this context, several studies have investigated the wrinkling mechanism. Driving forces for Gr wrinkling include (i) mismatch in strains [24] and/or

thermal expansion coefficients between Gr and the substrate [25], (ii) non-uniform interatomic/interfacial interactions [26], (iii) solvent trapping [6], and (iv) high solvent surface tension [8]. These insights have in turn led to the development of new routes to intentionally produce and manipulate wrinkles. For example, wrinkling and crumpling of large-area Gr can be achieved by transferring Gr film to pre-stretched elastomeric substrates [24], in which mismatch in strain determines the density, height, and pitch of the wrinkles. Mismatch in surface roughness and/or area has also been implemented to generate wrinkles by either transferring planar Gr onto a non-planar substrate or vice versa (e.g., growing corrugated Gr film on nanotextured Cu substrate and then transferring the Gr onto planar substrates) [27]. These approaches can generate a high density of wrinkles on Gr, conferring the resulting Gr with unique mechanical and optoelectronic characteristics. However, it remains a challenge to precisely control the position, orientation, and shape of the individual wrinkles.

Herein, we propose a new strategy to create wrinkles in a desired location and direction while suppressing wrinkle formation on unwanted regions, inspired by the spreading and wrinkling phenomena frequently found during wallpapering and/or ironing. To enable this, we introduced a regular array of holes in a Gr-based thin membrane [28,29], through which trapping and evaporation of solution between Gr and substrate surface were naturally regulated. This approach generated lattice patterns of Gr/Cu ripples and subsequently Gr wrinkles. Through electron microscopy and atomic force microscopy (AFM) investigation, wrinkles were found to connect neighboring holes, where

* Correspondence author.

E-mail address: wipark@hanyang.ac.kr (W.I. Park).<https://doi.org/10.1016/j.apsusc.2019.145184>

Received 25 September 2019; Received in revised form 19 November 2019; Accepted 24 December 2019

Available online 27 December 2019

0169-4332/ © 2019 Elsevier B.V. All rights reserved.

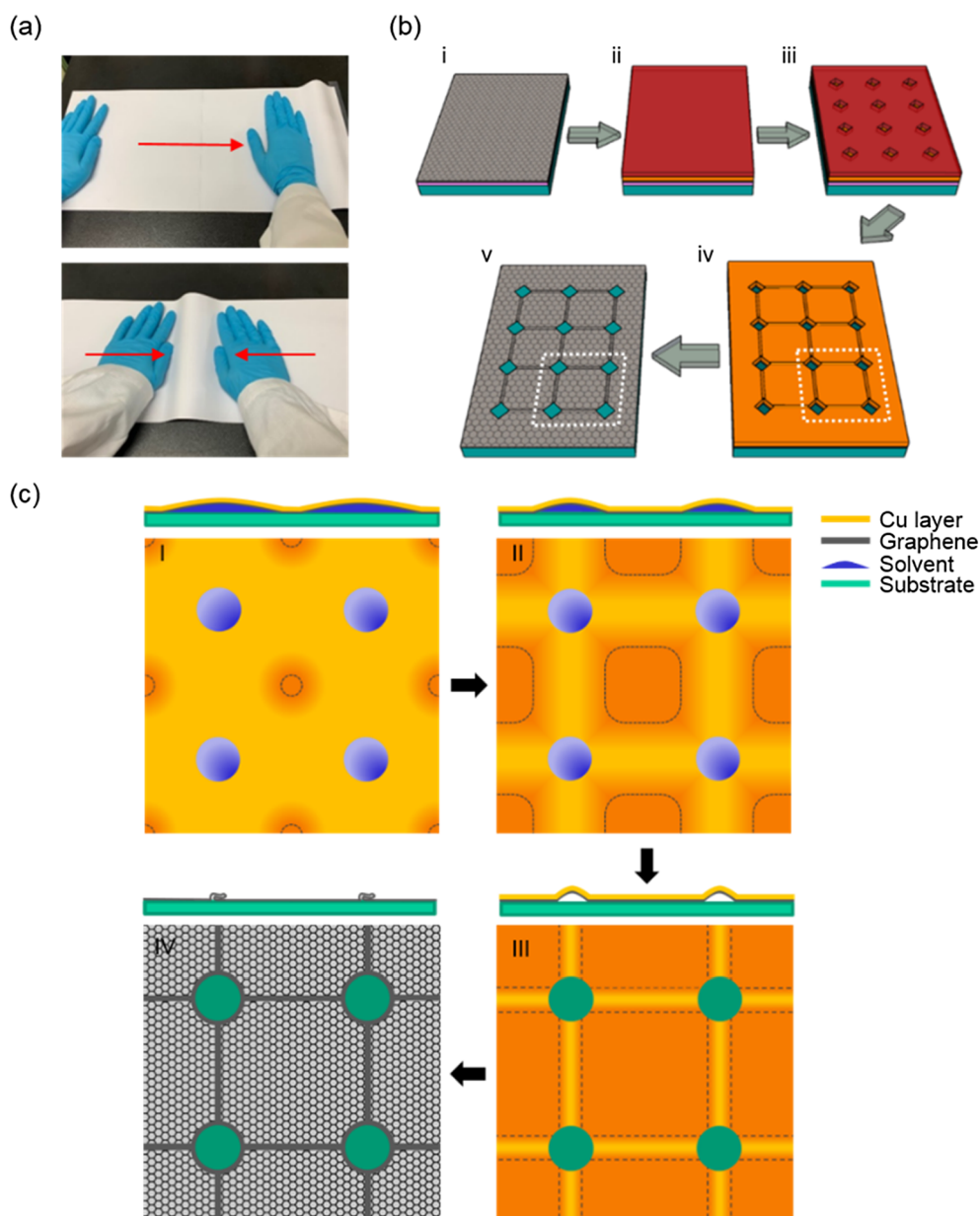


Fig. 1. Schematic illustration of Gr/Cu ripple and Gr wrinkle formation. (a) Photo images showing the basic concepts of spreading (up) and wrinkling (down). (b) Schematic of the fabrication process of a Gr/Cu ripple (i–iv) and Gr wrinkle (iv–v). (c) Schematic cross-sectional and top views of Gr/Cu rippling (I–III) and Gr wrinkling (III–IV) processes, corresponding to the dashed square region in (b).

each wrinkle consisted of a couple of folded layers with a width in the range of 300–500 nm and height in the range of 10–20 nm. The detailed wrinkling process and corresponding mechanism were characterized by correlating the size and shape of the linear Gr/Cu channel (hereafter referred to as ‘Gr/Cu ripple’) and Gr wrinkles with their mechanical behaviors (i.e., stress-strain behavior and recovery). Our approach is simple yet applicable to produce microscale lattice patterns of atomically thin membranes that are useful for diverse applications including highly localized resistive heater [22], nanochannels [30,31], foldable electrodes [32], and mechanical sensor array.

2. Experimental

2.1. CVD growth of Gr and flip-over transfer

Mostly single-layer Gr was synthesized on Cu foil (25 μm thickness, 99.999%, Alfa Aesar) by CVD using a previously developed method

[33,34]. In brief, a $1.5 \times 1.5 \text{ cm}^2$ square of Cu foil was placed in the center of CVD quartz tubular reactor (9 in.-diameter) that was then pumped to vacuum below 50 mtorr. The sample was thermally annealed at 1000 $^\circ\text{C}$ under 35 standard cubic centimeters per minute (SCCM) hydrogen gas flow for 20–30 min, and then a precursor of 15 SCCM methane gas flow was introduced to initiate Gr growth. During growth, the pressure was kept at 800 mtorr. After 10 min Gr growth, methane gas flow was turned off and the tube reactor was cooled down rapidly to room temperature. After the CVD process, the Gr film on the Cu foil was coated with a 400-nm thick poly methyl methacrylate (PMMA, C4) layer by spin-coating at 2500 rpm for 35 s. The thin Gr/PMMA membrane was then detached from the Cu foil in ammonium persulfate solution and the remaining Gr/PMMA sheet was rinsed with distilled (DI) water. The Gr/PMMA membrane was then transferred onto the target substrate (Si/SiO₂ substrate). During the transfer, the Gr/PMMA sheet was flipped over so that bare Gr surface faced upwards (Fig. 1b–i).

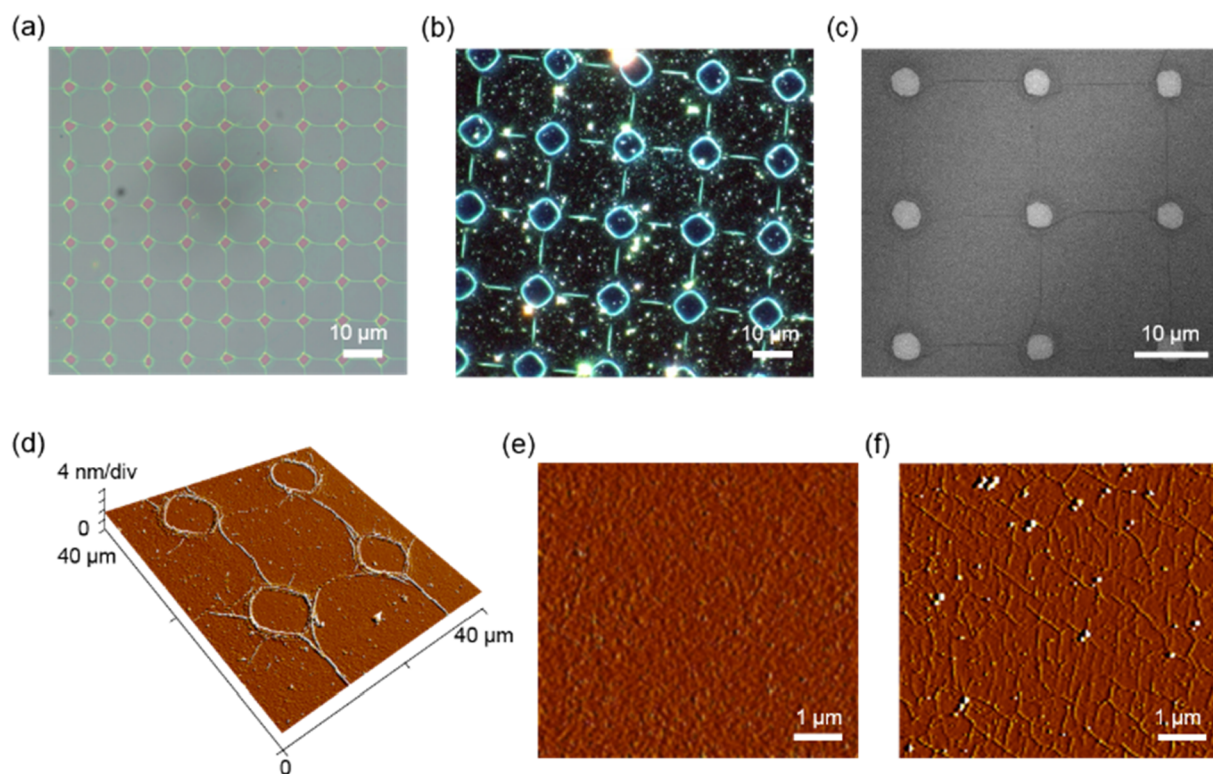


Fig. 2. Structural characterization of Gr wrinkles. (a) Bright field and (b) dark field OM images, (c) SEM image, and (d) 3D AFM image of the square lattice pattern of Gr wrinkles. Hole diameters/center-to-center distances: 2 $\mu\text{m}/10 \mu\text{m}$ (a), 8 $\mu\text{m}/20 \mu\text{m}$ (b), 4 $\mu\text{m}/16 \mu\text{m}$ (c) and 8 $\mu\text{m}/20 \mu\text{m}$ (d). (e) and (f) AFM images comparing the planar region surrounded by wrinkles in (d) and that of conventional wet-transferred Gr.

2.2. Fabrication of Gr/Cu ripples

A 40 nm-thick Cu thin film was deposited on the PMMA/Gr layer on the Si/SiO₂ substrate using a thermal evaporator. This was followed by coating with a 1.5 μm -thick photoresist (PR, AZ5214) layer using spin coating at 4000 rpm for 35 s. Next, a 2D array of holes with a diameter and center-to-center spacing in the range of 2–8 μm and 10–20 μm , respectively, was defined on the Gr/Cu/PR layer by photolithography followed by Cu etching with copper etchant and Gr etching by oxygen plasma at 30 W for 5 sec (Fig. 1b–ii and Fig. 1b–iii) [35]. After making the hole array, the specimen was placed in acetone. This process removed the top PR layer and simultaneously enabled the acetone to percolate down through the holes and dissolve the PMMA layer occupying the space between the Gr layer and SiO₂ substrate surface. After sufficient immersion in acetone to completely dissolve the PMMA layer (> 20 min), the specimen was moved to methanol, where the acetone between the Gr layer and SiO₂ was replaced by methanol. After keeping the specimen in methanol for more than 10 min, it was pulled out of the solvent and then naturally dried at room temperature. During this stage, Gr/Cu ripples interconnecting neighboring holes formed during the gradual evaporation of trapped methanol droplets (Fig. 1b–iv).

2.3. Fabrication of Gr wrinkles

After creating Gr/Cu ripples, the specimen was placed inside copper etchant to remove the top Cu layer, followed by rinsing in DI water and natural drying at room temperature. During this process, transformation from Gr/Cu ripples to Gr wrinkles, involving adhesion, folding, and collapse of Gr to the substrate surface, occurred.

3. Results and discussion

The basic concept of our approach is shown schematically in Fig. 1a. When wallpapering a wall, one can inhibit wrinkling by attaching one

side of the wallpaper and then gently spreading out the wallpaper so that the attached region gradually expands (Fig. 1a, top). This procedure can squeeze out trapped air and remaining glue adhesive between the wall and the paper, thereby preventing wrinkle formation. Meanwhile, if two opposite edges of paper are attached to the wall and the attached regions extend inward, a wrinkle develops at the place where both attached areas meet each other (Fig. 1a, bottom).

To mimic this phenomenon and control the wrinkling of Gr, we regulated the initiation of adhesion and spreading outwards of Gr-based thin membrane floating lightly in the solution above the substrate. Our approach to this is illustrated in Fig. 1b. First, CVD-grown single-layer Gr with a thin PMMA layer underneath was transferred onto Si/SiO₂ substrate (Fig. 1b–i). After coating of an ~40-nm thick Cu layer and PR on Gr, a 2–8 μm diameter hole array was defined on the Gr/Cu/PR layer (Fig. 1b–ii and Fig. 1b–iii) and subsequently, the PR layer was removed by immersing the specimen in acetone. This process enabled the acetone to percolate down through the holes and dissolve the PMMA layer underneath the Gr. The specimen was then placed immediately in methanol. During this stage, methanol replaced the acetone occupying the space between the Gr-based membrane and substrate. When the specimen was pulled out of the solution, the infiltrated methanol vaporized through the holes gradually, producing Gr/Cu ripples interconnecting the hole array (Fig. 1b–iv). Panels I–III in Fig. 1c highlight the ripple formation process. As the volume of trapped methanol decreased, each median of the surrounding four holes in each rectangle was first brought into close contact with the substrate (Fig. 1c, I), and the adhesion region expanded gradually until a certain size (height and width) of Gr/Cu ripples developed (Fig. 1c, II). This Gr/Cu ripple was maintained even after complete evaporation of the trapped acetone (Fig. 1c, III). Finally, the sample was immersed in copper etching solution to remove the copper film on Gr, followed by rinsing in DI water (Fig. 1b–v). During this stage, a complicated form of Gr wrinkles was generated through adhesion, folding, and collapse of Gr to the substrate surface (Fig. 1c, IV).

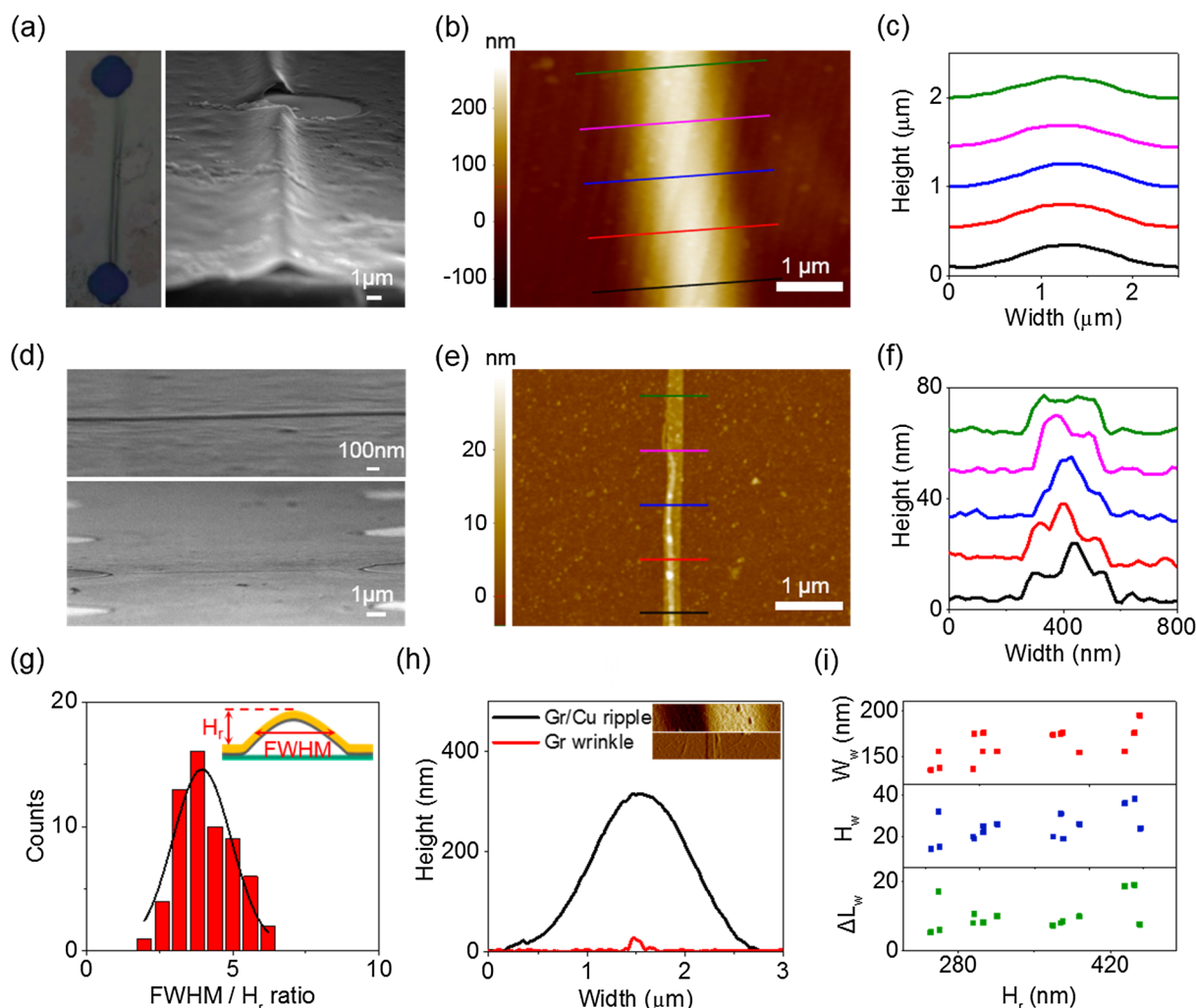


Fig. 3. Analysis of Gr/Cu ripples and Gr wrinkles. (a) OM and tilted-view SEM images of a Gr/Cu ripple. (b) AFM image and (c) corresponding height-profiles of a Gr/Cu ripple. (d) Low-magnification (bottom) and high-magnification (top) SEM images of a Gr wrinkle. (e) AFM image and (f) corresponding height-profiles of a Gr wrinkle. (g) Histogram of FWHM to height (H_r) ratio of Gr/Cu ripples. (h) Overlap of height versus width curves for Gr/Cu ripples and Gr wrinkles. (i) Width W_w , height H_w , and stretched length ΔL_w of Gr wrinkles according to the height of the Gr/Cu ripples.

Bright field and dark field optical microscopy (OM) images in Fig. 2a, b show the square lattice pattern of Gr wrinkles, with 10 μm (a) and 20 μm (b) periods, that developed over a large area. Most wrinkles were straight and interconnected the hole array only along vertical or horizontal directions. Scanning electron microscopy (SEM) images confirmed that the actual width of the wrinkles was about 300–500 nm (Fig. 2c and Fig. S1). We further performed non-contact AFM analysis to determine the fine 3D features of the wrinkles between the holes (Fig. 2d). Width was similar to that measured from SEM images, indicating no significant tip convolution effect in our AFM measurement. The height of the wrinkles was about 10–20 nm. AFM image also revealed that in addition to linear wrinkles, circular wrinkles were present along the rims of holes. X-ray photoelectron spectroscopy (XPS) spectra showed a dominant C 1s peak at 284 eV corresponding mainly to C–C, although an O 1s signal from the substrate was present at 532 eV, indicating that both wrinkle and planar layers were Gr (Fig. S2) [36,37]. In addition, no Cu 2s peak was present, indicating that our wrinkling process leaves no significant Cu residue. The C 1s spectrum can be deconvoluted into four sub-peaks. The two dominant peaks at 284 and 285 eV are generally observed in graphene, and can be assigned to sp^2 hybridized C atoms in graphene and sp^3 hybridized C atoms of amorphous carbon or C–H bonds of graphene, respectively [38]. On the other hand, the other peaks at 286 and 288 eV is assigned

to C=O and O–C=O peak of PMMA residue. It is noted that similar levels of the PMMA peaks were observed in the graphene even after removing the PMMA by 120 min dip in acetone [38].

It is important to note that our method suppressed wrinkle formation on the planar regions surrounded by wrinkles, which is analogous to ironing out wrinkles from clothes (Fig. 2e). In the case of Gr obtained by the conventional wet-transfer method, a high density of surface corrugations (wrinkles and ripples) 2 nm in height and 150 nm in width was observed over almost the entire area (Fig. 2f). In contrast, the wrinkle-free region in Fig. 2e exhibited a relatively flat surface with a root mean square roughness (RMS) value of 0.73 nm, which is much lower than the RMS value (1.53 nm) of conventional wet-transferred Gr. This result indicates that during gradual expansion of the adhered layer, wrinkle was not just suppressed, but intrinsic wrinkles actually unfolded.

To confirm the validity of our proposed wrinkling mechanism, we conducted additional microscopic analysis. First, we performed in-situ investigation of Gr/Cu ripple formation under OM (Fig. S3). As the trapped methanol vaporized gradually, the Gr/Cu membrane started to sink down and adhere to the substrate from the centers of four neighboring holes, as noted by the change from irregular multiple colors to a uniform reddish color. In addition, ripple formation was identified by the appearance of straight lines connecting the holes (Fig. S3, $t \geq 49$ s).

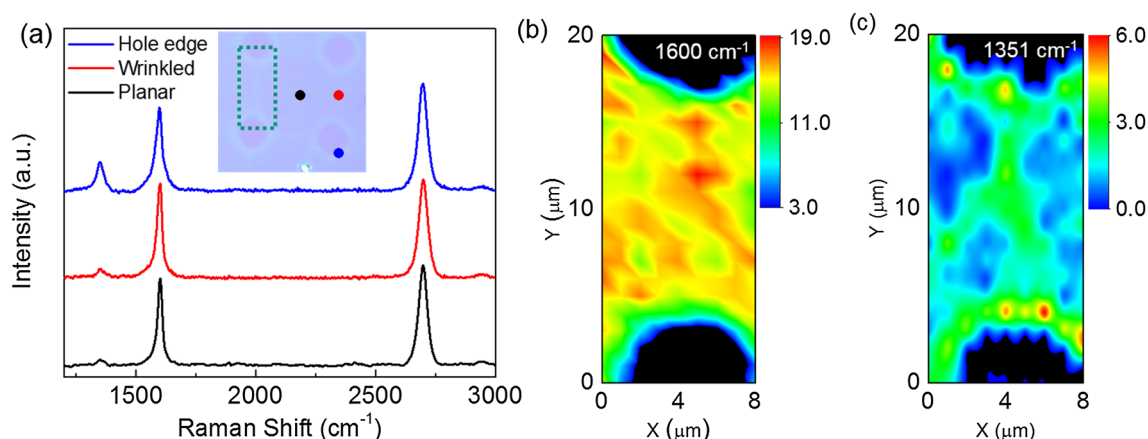


Fig. 4. Raman spectroscopy analysis. (a) Raman spectra from different regions of Gr in the OM image (inset): circular edge (blue), wrinkled (red) and planar (black) regions. (b) and (c) Raman mapping images of the G peak (1600 cm^{-1}) and D peak ($\sim 1351\text{ cm}^{-1}$), collected at the dotted square area of the OM image shown in the inset of (a).

This Gr/Cu ripple was maintained even after complete evaporation of the trapped methanol (Fig. 3a, left). This experimental observation is consistent with our model of the ripple formation process.

Tilted-view SEM image obtained by zooming in on the Gr/Cu ripples interconnecting the holes revealed the formation of a straight hollow channel with micrometer-scale width and height. Meanwhile, the rims of holes remained flat until this stage (Fig. 3a). More detailed morphological information (i.e., width, height, contact angle) about the Gr/Cu ripples was obtained through AFM analysis (Fig. 3b). We found that the size of individual ripples varied over a wide range depending on diverse variables such as the size, spacing, and arrangement of holes (the width of ripple W_r was generally in the range of 2–4 μm for a 2D array of holes, while W_r increased up to $\sim 6\text{ }\mu\text{m}$ for a 1D array of holes). However, each ripple had a uniform width and height (Fig. 3c). Interestingly, measurements of the ripples at many different places in a sample and in different samples revealed that most ripples had a similar aspect ratio (full width at half maximum FWHM to height H_r , ratio of 3.8 ± 1.8) as well as cross-sectional shape (Fig. 3g). We hypothesized that the size of the ripples was likely determined by tensile strength and recovery while the aspect ratio and shape of the ripple were determined by interfacial interactions and plastic deformation. The corresponding stress-strain behaviors are illustrated schematically in Fig. S4. The tensile stress accompanied by permeation of solution induced elastic deformation and plastic deformation (after yielding point 2) in sequence (from points 1 to 3 in Fig. S4). Upon gradual release of the trapped methanol, elastic strain recovered (from points 3 to 5 in Fig. S4). At point 5, when the trapped droplet disappeared completely, only plastic deformation remained and determined the overall length of the ripple L (i.e., $L = \Delta L_p + L_0$, where ΔL_p is the plastic deformation length and L_0 is the initial length that is equal to the W_r). Simple calculation showed that the strain of the ripple in Fig. 3b was 0.007, which is over 10 times greater than the strain at yielding (~ 0.0008) [39]. At point 5, the ripple adopted its final shape during replacement of the methanol droplet by air, in which the interplay between interfacial energies and plastic deformation energy played an important role in determining the aspect ratio and curved shape of the ripple.

As a final stage, Gr wrinkles were generated when the Cu layer was removed by Cu etchant (Fig. 3d). AFM analysis showed that the Gr wrinkles had a complicated form, and their width and height were significantly smaller than those of Gr/Cu ripples. The discrepancy in size between Gr/Cu ripples and Gr wrinkles was made clear by superimposing the AFM height-profiles of ripple and wrinkle before and after Cu etching (Fig. 3h). This discrepancy is due to the different deformation behaviors of Gr and Cu. Gr exhibits dominant elastic deformation in stress-strain behavior until fracture occurs [40,41]. Importantly,

even after considerable yielding of the Cu layer in the Gr/Cu ripple, the Gr layer underneath was still in an elastically elongated condition. Accordingly, upon the dissolution of Cu, the Gr in the liquid underwent elastic recovery. During this stage, additional expansion of the Gr layer's adhesion to the substrate surface together with folding, merging, and collapse occurred, producing the final form of the complicated Gr wrinkles (Fig. 3f). Statistical analysis of height and width differences between Gr/Cu ripples and Gr wrinkles showed that the height H_w and width W_w of wrinkles decreased more than 10-fold. Interestingly, W_w increased with the size of the ripple (i.e., H_r) while H_w was independent of the size of ripple, but was affected by the degree of folding. When only the cross-sectional contour was considered, elongation of wrinkle ΔL_w , which was determined by the difference between cross-sectional length and width of each wrinkle, was also independent of H_r . We therefore concluded that Gr was almost recovered and that the accumulation of intrinsic surface corrugations resulted in the ΔL_w of wrinkles at the final stage.

To investigate structural changes before and after wrinkling, we performed Raman spectroscopy measurements. Representative Raman spectra achieved with a $\sim 1\text{ }\mu\text{m}$ diameter laser beam (a 532 nm excitation) focused on different regions of Gr, as marked by circles in optical image (inset), are shown in Fig. 4a. Both planar and wrinkled regions exhibited distinct 2D and G peaks at $\sim 2698\text{ cm}^{-1}$ and $\sim 1600\text{ cm}^{-1}$, respectively, with the 2D and G peak intensity ratio higher than 1 ($I_{2D}/I_G = \sim 1.4$) [42]. This result suggests that Gr was composed mostly of single layer Gr, and even after wrinkling, there was no significant tight oscillation of the Gr layers [43]. The intensity of the D peak ($\sim 1351\text{ cm}^{-1}$), which is associated with defects and lattice distortions in Gr [44], increased slightly but was maintained at low levels after wrinkling, as similar to that of wet-transferred graphene (Fig. S5). Spectra measured at different positions exhibited similar features (Fig. S6), with an average I_{2D}/I_G ratio of 1.13 and 1.24 and an I_D/I_G ratio of 0.08 and 0.13 for planar and wrinkled regions, respectively. However, D peak intensity increased suddenly at the edges of the holes, often by more than four-fold, which is attributed to carbon disorders caused by oxygen plasma etching (Fig. 4a blue line) [45]. The similar Raman characteristics of Gr and Gr wrinkles were further supported by Raman mapping images (Fig. 4b and c). It is important to note that large shifts of the G and 2D peaks were observed from graphene bubbles under tensile strain [46]. However, in our case, there is no noticeable difference in the G and 2D peak positions between the graphene regions and wrinkled regions. Considering all these Raman results, we suggest that Gr wrinkles fully recovered to a stress-free state and thereby maintained the intrinsic high structural quality of Gr, in good agreement with the stress-strain behavior results.

4. Conclusions

We demonstrated a new and robust approach to generate a regular pattern of Gr wrinkles. Analogous to wallpapering and/or ironing, our approach produces straight wrinkles in a desired location and direction, while suppressing surface corrugations on the region surrounded by wrinkles. Raman spectroscopy measurements showed that the Gr wrinkles maintained the intrinsic defect- and stress-free state and high structural quality of Gr. This study advances understanding of wrinkle formation at the atomically-thin limit, and our approach can be used to produce artificially controlled wrinkles that confer atomically-thin materials with novel functionalities.

CRedit authorship contribution statement

Sang Il Lee: Methodology, Writing - original draft, Visualization. **Hyeong-Gyu Lim:** Formal analysis, Software. **Sun Sang Kwon:** Methodology, Software. **Su Han Kim:** Investigation, Data curation. **Jae Hyung Lee:** Validation, Formal analysis. **Jeong-Min Park:** Formal analysis, Resources. **Jae-il Jang:** Formal analysis, Investigation. **Sung Ik Yang:** Formal analysis, Investigation. **Won Il Park:** Conceptualization, Writing - original draft, Writing - review & editing, Supervision.

Declaration of Competing Interest

The authors declare that they have no known competing financial interests or personal relationships that could have appeared to influence the work reported in this paper.

Acknowledgements

This work was supported by the National Research Foundation of Korea funded by the Ministry of Science, ICT and Future Planning of Korea (No. 2018R1A2B2006410), the AFOSR/AOARD, USA (FA2386-18-1-4110) and the Human Resources Program in Energy Technology of the Korea Institute of Energy Technology Evaluation and Planning (KETEP), granted financial resource from the Ministry of Trade, Industry & Energy, Republic of Korea. (No. 20174030201750)

Appendix A. Supplementary material

Supplementary data to this article can be found online at <https://doi.org/10.1016/j.apsusc.2019.145184>.

References

- W.J. Chen, X.C. Gui, L.L. Yang, H. Zhu, Z.K. Tang, Wrinkling of two-dimensional materials: methods, properties and applications, *Nanoscale Horiz.* 4 (2019) 291–320.
- X. Meng, M. Li, Z. Kang, X. Zhang, J. Xiao, Mechanics of self-folding of single-layer graphene, *J. Phys. D: Appl. Phys.* 46 (2013) 055308.
- N. Liu, Z. Pan, L. Fu, C. Zhang, B. Dai, Z. Liu, The origin of wrinkles on transferred graphene, *Nano Res.* 4 (2011) 996.
- C.G. Wang, Y.P. Liu, L. Lan, H.F. Tan, Graphene wrinkling: formation, evolution and collapse, *Nanoscale* 5 (2013) 4454–4461.
- D. Yoon, Y.-W. Son, H. Cheong, Negative thermal expansion coefficient of graphene measured by Raman spectroscopy, *Nano Lett.* 11 (2011) 3227–3231.
- V.E. Calado, G.F. Schneider, A.M.M.G. Theulings, C. Dekker, L.M.K. Vandersypen, Formation and control of wrinkles in graphene by the wedging transfer method, *Appl. Phys. Lett.* 101 (2012) 103116.
- J.-K. Choi, J. Kwak, S.-D. Park, H.D. Yun, S.-Y. Kim, M. Jung, S.Y. Kim, K. Park, S. Kang, S.-D. Kim, D.-Y. Park, D.-S. Lee, S.-K. Hong, H.-J. Shin, S.-Y. Kwon, Growth of wrinkle-free graphene on texture-controlled platinum films and thermal-assisted transfer of large-scale patterned graphene, *ACS Nano* 9 (2015) 679–686.
- H.H. Kim, S.K. Lee, S.G. Lee, E. Lee, K. Cho, Wetting-assisted crack- and wrinkle-free transfer of wafer-scale graphene onto arbitrary substrates over a wide range of surface energies, *Adv. Funct. Mater.* 26 (2016) 2070–2077.
- M. Kim, P. Kang, J. Leem, S. Nam, A stretchable crumpled graphene photodetector with plasmonically enhanced photoresponsivity, *Nanoscale* 9 (2017) 4058–4065.
- P. Kang, M.C. Wang, P.M. Knapp, S. Nam, Crumpled graphene photodetector with enhanced, strain-tunable, and wavelength-selective photoresponsivity, *Adv. Mater.* 28 (2016) 4639–4645.
- A. Krishna, J.M. Kim, J. Leem, M.C. Wang, S. Nam, J. Lee, Dynamic Radiative Thermal Management by Crumpled Graphene, in: 2019 18th IEEE Intersociety Conference on Thermal and Thermomechanical Phenomena in Electronic Systems (ITherm), 2019, pp. 797–802.
- H. Lim, J. Jung, R.S. Ruoff, Y. Kim, Structurally driven one-dimensional electron confinement in sub-5-nm graphene nanowrinkles, *Nat. Commun.* 6 (2015) 8601.
- W. Yan, W.-Y. He, Z.-D. Chu, M. Liu, L. Meng, R.-F. Dou, Y. Zhang, Z. Liu, J.-C. Nie, L. He, Strain and curvature induced evolution of electronic band structures in twisted graphene bilayer, *Nat. Commun.* 4 (2013) 2159.
- C. Si, Z.M. Sun, F. Liu, Strain engineering of graphene: a review, *Nanoscale* 8 (2016) 3207–3217.
- J. Martin, N. Akerman, G. Ulbricht, T. Lohmann, J.H. Smet, K. von Klitzing, A. Yacoby, Observation of electron-hole puddles in graphene using a scanning single-electron transistor, *Nat. Phys.* 4 (2007) 144.
- R.J.T. Nicholl, H.J. Conley, N.V. Lavrik, I. Vlasiouk, Y.S. Puzryev, V.P. Sreenivas, S.T. Pantelides, K.I. Bolotin, The effect of intrinsic crumpling on the mechanics of free-standing graphene, *Nat. Commun.* 6 (2015) 8789.
- J.-Y. Hong, W. Kim, D. Choi, J. Kong, H.S. Park, Omnidirectionally stretchable and transparent graphene electrodes, *ACS Nano* 10 (2016) 9446–9455.
- D.W. Boukhvalov, M.I. Katsnelson, Enhancement of chemical activity in corrugated graphene, *J. Phys. Chem. C* 113 (2009) 14176–14178.
- W. Chen, X. Gui, S. Li, L. Yang, B. Liang, H. Zhu, J. She, Z. Tang, Fabrication of wrinkled graphene based on thermal-enhanced Rayleigh-Bénard convection for field electron emission, *Carbon* 129 (2018) 646–652.
- S.K. Nemani, D. Chen, M.H. Mohamed, H. Sojoudi, Stretchable and hydrophobic electrochromic devices using wrinkled graphene and PEDOT:PSS, *J. Nanomater.* 2018 (2018) 10.
- H. Nakajima, T. Morimoto, Y. Okigawa, T. Yamada, Y. Ikuta, K. Kawahara, H. Ago, T. Okazaki, Imaging of local structures affecting electrical transport properties of large graphene sheets by lock-in thermography, *Sci. Adv.* 5 (2019) eaau3407.
- K.L. Grosse, V.E. Dorgan, D. Estrada, J.D. Wood, I. Vlasiouk, G. Eres, J.W. Lyding, W.P. King, E. Pop, Direct observation of resistive heating at graphene wrinkles and grain boundaries, *Appl. Phys. Lett.* 105 (2014) 143109.
- C. Wang, Y. Liu, L. Li, H. Tan, Anisotropic thermal conductivity of graphene wrinkles, *Nanoscale* 6 (2014) 5703–5707.
- J. Zang, S. Ryu, N. Pugno, Q. Wang, Q. Tu, M.J. Buehler, X. Zhao, Multifunctionality and control of the crumpling and unfolding of large-area graphene, *Nat. Mater.* 12 (2013) 321.
- S.J. Chae, F. Güneş, K.K. Kim, E.S. Kim, G.H. Han, S.M. Kim, H.-J. Shin, S.-M. Yoon, J.-Y. Choi, M.H. Park, C.W. Yang, D. Pribat, Y.H. Lee, Synthesis of large-area graphene layers on poly-nickel substrate by chemical vapor deposition: wrinkle formation, *Adv. Mater.* 21 (2009) 2328–2333.
- W. Chen, X. Gui, B. Liang, M. Liu, Z. Lin, Y. Zhu, Z. Tang, Controllable fabrication of large-area wrinkled graphene on a solution surface, *ACS Appl. Mater. Interfaces* 8 (2016) 10977–10984.
- Z. Pan, N. Liu, L. Fu, Z. Liu, Wrinkle engineering: a new approach to massive graphene nanoribbon arrays, *J. Am. Chem. Soc.* 133 (2011) 17578–17581.
- Z. Qin, M. Taylor, M. Hwang, K. Bertoldi, M.J. Buehler, Effect of wrinkles on the surface area of graphene: toward the design of nanoelectronics, *Nano Lett.* 14 (2014) 6520–6525.
- M. Becton, X. Wang, Tailoring patterns of graphene wrinkles by circular torsion, *Appl. Surf. Sci.* 363 (2016) 13–20.
- R. Fan, R. Karnik, M. Yue, D. Li, A. Majumdar, P. Yang, DNA Translocation in Inorganic Nanotubes, *Nano Lett.* 5 (2005) 1633–1637.
- Y.H. Zhang, Q. Fu, Y. Cui, R.T. Mu, L. Jin, X.H. Bao, Enhanced reactivity of graphene wrinkles and their function as nanosized gas inlets for reactions under graphene, *Phys. Chem. Chem. Phys.* 15 (2013) 19042–19048.
- W.-K. Lee, J. Kang, K.-S. Chen, C.J. Engel, W.-B. Jung, D. Rhee, M.C. Hersam, T.W. Odom, Multiscale, hierarchical patterning of graphene by conformal wrinkling, *Nano Lett.* 16 (2016) 7121–7127.
- S.S. Kwon, J. Yi, W.W. Lee, J.H. Shin, S.H. Kim, S.H. Cho, S. Nam, W.I. Park, Reversible and irreversible responses of defect-engineered graphene-based electrolyte-gated pH sensors, *ACS Appl. Mater. Interfaces* 8 (2016) 834–839.
- S.H. Kim, J.H. Lee, J.S. Park, M.S. Hwang, H.G. Park, K.J. Choi, W. Il Park, Performance optimization in gate-tunable Schottky junction solar cells with a light transparent and electric-field permeable graphene mesh on n-Si, *J Mater Chem C* 5 (2017) 3183–3187.
- S.S. Kwon, J.H. Shin, J. Choi, S. Nam, W.I. Park, Defect-mediated molecular interaction and charge transfer in graphene mesh-glucose sensors, *ACS Appl. Mater. Interfaces* 9 (2017) 14216–14221.
- H. Huang, Y. Xia, X.Y. Tao, J. Du, J.W. Fang, Y.P. Gan, W.K. Zhang, Highly efficient electrolytic exfoliation of graphite into graphene sheets based on Li ions intercalation-expansion-microexplosion mechanism, *J. Mater. Chem.* 22 (2012) 10452–10456.
- F.T. Johra, J.-W. Lee, W.-G. Jung, Facile and safe graphene preparation on solution based platform, *J. Ind. Eng. Chem.* 20 (2014) 2883–2887.
- G. Cunge, D. Ferrah, C. Petit-Etienne, A. Davydova, H. Okuno, D. Kalita, V. Bouchiat, O. Renault, Dry efficient cleaning of poly-methyl-methacrylate residues from graphene with high-density H₂ and H₂-N₂ plasmas, *J. Appl. Phys.* 118 (2015) 123302.
- T.A. Ring, P. Feeney, D. Boldridge, J. Kasthurirangan, S.T. Li, J.A. Dirksen, Brittle and ductile fracture mechanics analysis of surface damage caused during CMP, *J. Electrochem. Soc.* 154 (2007) H239–H248.
- C. Daniels, A. Horning, A. Phillips, D.V.P. Massote, L. Liang, Z. Bullard,

- B.G. Sumpter, V. Meunier, Elastic, plastic, and fracture mechanisms in graphene materials, *J. Phys.: Condens. Matter* 27 (2015) 373002.
- [41] Y. Park, S. Hyun, Effects of Grain Size Distribution on the Mechanical Properties of Polycrystalline Graphene, *J. Korean Ceram. Soc* 54 (2017) 506–510.
- [42] L.M. Malard, M.A. Pimenta, G. Dresselhaus, M.S. Dresselhaus, Raman spectroscopy in graphene, *Phys. Rep.* 473 (2009) 51–87.
- [43] Z. Ni, Y. Wang, T. Yu, Y. You, Z. Shen, Reduction of Fermi velocity in folded graphene observed by resonance Raman spectroscopy, *Phys. Rev. B* 77 (2008) 235403.
- [44] J.H. Shin, S.H. Kim, S.S. Kwon, W.I. Park, Direct CVD growth of graphene on three-dimensionally-shaped dielectric substrates, *Carbon* 129 (2018) 785–789.
- [45] I. Childres, L.A. Jauregui, J. Tian, Y.P. Chen, Effect of oxygen plasma etching on graphene studied using Raman spectroscopy and electronic transport measurements, *New J. Phys.* 13 (2011) 025008.
- [46] J. Zabel, R.R. Nair, A. Ott, T. Georgiou, A.K. Geim, K.S. Novoselov, C. Casiraghi, Raman spectroscopy of graphene and bilayer under biaxial strain: bubbles and balloons, *Nano Lett.* 12 (2012) 617–621.